

Tutorial on nanostructured superconductors

1 Introduction

Superconductivity represents an extraordinary phenomenon. In the superconducting state the material not only exhibits no electric resistance to an applied DC current, it shows also unique properties in magnetic fields that can be used for a large variety of applications ranging from energy production and management, medical diagnostics, to sensor and information technology. For a long time the application of superconductivity was hampered by its low transition temperature T_c that required cooling down to liquid He temperature at 4.2 K. As a consequence, superconductive solutions were considered and developed in the past only if classical solutions were not feasible. This was (and still is) the case for medical applications like magnetic resonance imaging (MRI) or electroencephalography, particle accelerators, and special detectors (e.g., bolometers or highly sensitive magnetic field detectors).

With the discovery of the so-called high- T_c materials with T_c values of 90 K and higher (see Figure 1), this situation has changed. Now it was possible to attain the superconducting state with much cheaper cooling by liquid nitrogen. However, it soon turned out that the new superconductors (i) have a very complex crystallographic structure, (ii) are highly anisotropic (2D superconductivity), and (iii) possess superconducting parameters that allow even smallest inhomogeneities to reduce or even destroy the superconductivity locally.

As a result, it is essential to analyze, understand and, if possible, optimize superconductors at the nanoscale. This includes among others a detailed study of the nanostructure of these superconductors, the resulting ‘nanophysics’, and the impact of nanostructures introduced by nanopatterning on the superconducting properties. This book represents a detailed report on this activity that was performed in the framework of a European project, the COST Action MP1201 ‘*Nanoscale Superconductivity (NanoSC), Novel Functionalities through Optimized Confinement of Condensate and Fields*’.

2 A brief history of superconductivity

In 1908, Kamerlingh Onnes [1] succeeded in the liquefaction of helium with a boiling point of 4.2 K at atmospheric pressure. Since the boiling point can be reduced by pressure reduction, he was now able to extend the experimentally available tempera-

ture range towards absolute zero. Using this opportunity, he started an investigation of the electric resistance of metals. At that time, it was known that electrons are responsible for charge transport. However, different ideas about the mechanism of the electric conduction and the resulting temperature dependence of the resistance were discussed:

1. At low temperature the crystal lattice ‘freezes’ and the electrons are not scattered any longer. As a consequence the resistance of all metals would approach zero with decreasing temperature (Dewar, 1904).
2. Similar to option 1, however due to impurities in the lattice, the resistance would approach a finite limiting value (Matthiesen, 1864).
3. In contrast to option 1 and 2, the electrons could be ‘frozen’ (i.e., bound to their respective atoms) at low temperature. Consequently, the resistance would pass through a minimum and approach infinity at very low temperatures (Lord Kelvin, 1902).

Initially, Kamerlingh Onnes studied platinum and gold samples, which he could obtain already with high purity. He found that the experiment agreed with the second option. At zero temperature the electric resistance of these samples saturated at a finite limiting value, the so-called residual resistance, that depended upon the purity of the samples. The purer the samples, the smaller the residual resistance. However, Kamerlingh Onnes expected that, ideally, pure platinum or gold should have a vanishingly small resistance (first option).

In order to test this hypothesis, Kamerlingh Onnes decided to study mercury, the only metal that at that time could be highly purified via multiple distillation processes. He expected that the resistance of pure mercury would hardly be measurable at 4.2 K and that it would gradually approach zero resistance at even lower temperatures. The initial experiments seemed to confirm these concepts, i.e., below 4.2 K the resistance of mercury became immeasurably small (see Figure 1). However, he soon recognized that the observed effect could not be identified with the expected decrease of resistance. The resistance change resembled more a resistance jump within a few hundredths of a Kelvin than a continuous decrease (see Figure 1). Therefore, Kamerlingh Onnes stated that ‘*At this point (slightly below 4.2 K) ... Mercury had passed into a new state, which on account of its extraordinary electrical properties may be called the superconductive state*’ [2]. The new phenomenon was discovered and named superconductivity.

Meanwhile we know that superconductivity represents a widespread phenomenon. Many elements of the periodic system are superconductors (with Nb representing the element with the highest T_c of about 9.2 K) and thousands of superconducting compounds have been discovered in the meantime ranging from metallic compounds and oxides, to organic molecules (see Figure 1).

For the first 75 years, superconductivity represented a low-temperature phenomenon with the highest T_c of about 23.2 K in the A15 compound Nb₃Ge. In 1986

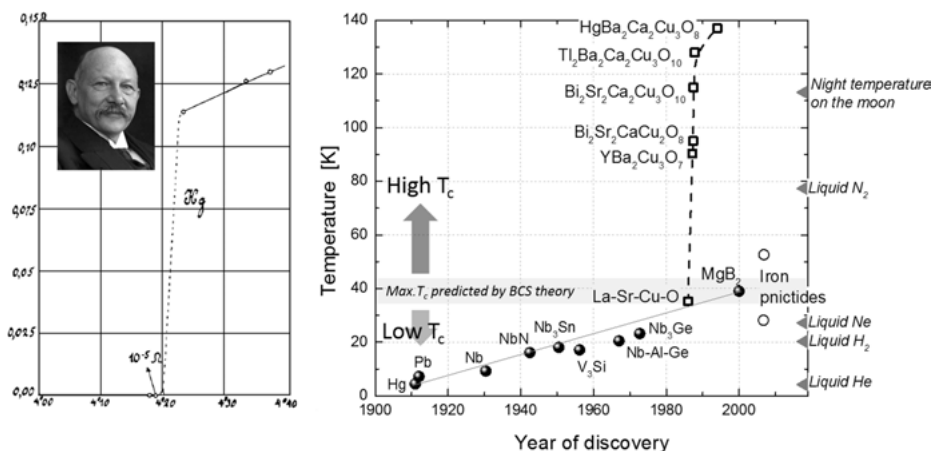


Fig. 1: Superconductivity of mercury (copy of the original figure from Kamerlingh Onnes [image in the figure]) and the evolution of the superconducting transition temperature T_c with time.

this changed, when Bednorz and Müller discovered superconductivity with a T_c in the range of 30 K in the copper-oxide system Ba-La-Cu-O [3]. This immediately started a ‘rush’ for new superconductors with even higher T_c ’s. Already in 1987, transition temperatures above 80 K were observed in the Y-Ba-Cu-O system [4]. During this time, new results more often were reported in press conferences than in scientific journals, the media carefully reported on these developments since superconductivity at temperatures above the boiling point of liquid nitrogen ($T = 77$ K) suggested many possible technical applications for this phenomenon.

Today, a large number of different Cu-O based (cuprate) superconductors with high transition temperatures are known, the so called ‘high- T_c superconductors’. The most studied high- T_c cuprates are YBa₂Cu₃O₇ (YBCO), their rare earth counterparts ReBa₂Cu₃O₇ (with Re = Sc, Ce, La, Nd, Sm, Eu, Gd, Dy, Ho, Er, Tm, Yb, Lu), and Bi₂Sr₂CaCu₂O₈ (BSCCO or Bi2212) with transition temperatures slightly above 90 K. The record T_c value is presently that of HgBa₂Ca₂Cu₃O₈, with a T_c of 135 K or 164 K at atmospheric pressure or a pressure of 30 GPa, respectively.

Surprisingly, only in 2000 superconductivity with a T_c of 39 K was detected in MgB₂, even though this compound represents a ‘classical’ metallic superconductor and had already been commercially available for a long time [5]. In 2008 superconductivity was detected in quite exotic compounds, the so-called iron pnictides [6]. In analogy to the copper oxide layers in the cuprates, in these material FeAs layers form the basic building block for the superconductivity. Compositions like LaFeAsO_{1-x}F_x, Ba_{1-x}K_xFe₂As₂, or ReFeAsO_{1-x} (with Re = Sm, Nd, Pr, Ce, La) show impressive T_c ’s up to 55 K. Finally, a large number of organic molecules also become superconducting at low temperature. Already in 1979 K. Bechgaard synthesized the first organic superconductor, (TMTSF)₂PF₆, with a T_c of 1.1 K at a pressure of 6.5 kbar. The correspond-

ing material class was later named after him. Nowadays, transition temperatures of up to 33 K (2007, alkali-doped fullerene $\text{RbCs}_2\text{C}_{60}$) have been achieved. Organic superconductors are of special interest since they can form quasi-2D or even quasi-1D structures like Fabre or Bechgaard salts (e.g., $\kappa\text{-BEDT-TTF}_2\text{X}$ or $\lambda\text{-BETS}_2\text{X}$ compounds), or graphite intercalation compounds.

This brief survey of superconductivity demonstrates that there has been a tremendous improvement of the transition temperature in the past years, which, however, is accompanied by a higher complexity and anisotropy of the material. The analysis, understanding, and optimization of the superconductivity in these materials clearly has to happen at the nanoscale.

3 Specific properties of superconductors

The most prominent property of the superconducting state is definitely the disappearance of the DC electric resistance (see Figure 1). The superconductor becomes an *ideal conductor*.

However, just as important is the behavior of the superconductor in magnetic fields. In 1933 Meissner and Ochsenfeld discovered that an externally applied magnetic field can be expelled from the interior of a superconductor (Figure 2), i.e., the superconductor can also act as an *ideal diamagnet* [28]. This can nicely be demonstrated in levitation experiments and represents the basis for levitation applications of superconductivity like levitation trains or magnetic bearings (Figure 2). Generally, the Meissner–Ochsenfeld effect is very surprising, since according to the induction law an ideal conductor is expected to preserve an interior constant magnetic field but not expel it. As will be shown later in this tutorial (Section 4.3), the behavior of a superconductor in a magnetic field is far more complex. It represents one of the major themes of this book.

4 Theoretical understanding

4.1 Microscopic approach of Bardeen, Cooper, and Schrieffer

The explanation for the unusual behavior of superconductors came with the BCS theory that was introduced by Bardeen, Cooper, and Schrieffer in 1957 [7]. They recognized that at the transition to the superconducting state, electrons (fermions) pairwise condense to a bosonic state, in which they form a coherent matter wave with a well-defined quantum-mechanic phase, the so-called Bose–Einstein condensate (the latter explains the Josephson effect that is introduced in the next section). They assumed that the interaction of the electrons is mediated by vibrations of the crystal lattice, i.e.,

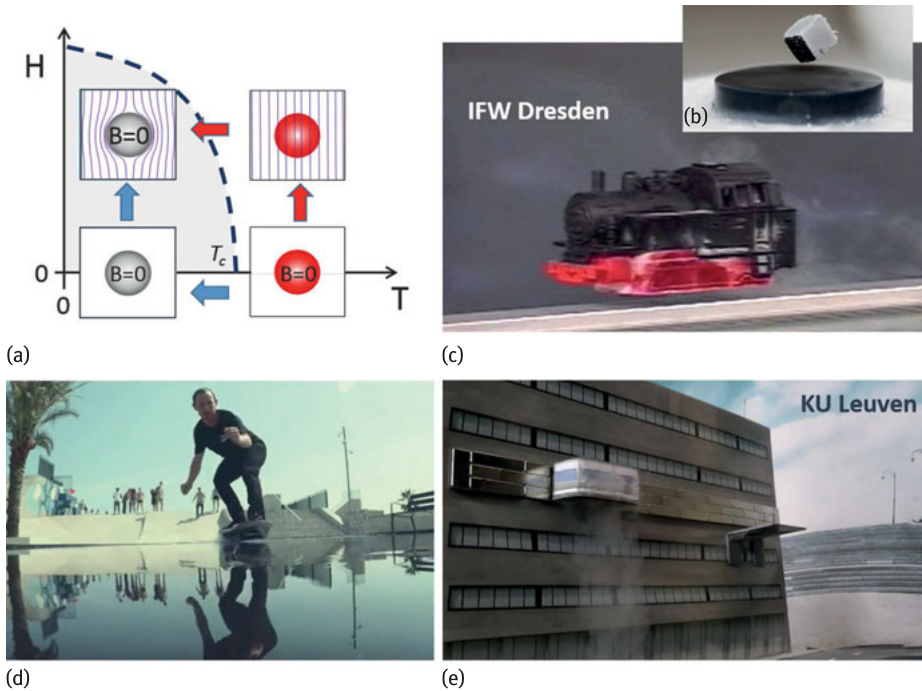


Fig. 2: (a) H-T phase diagram showing how a magnetic field interacts with a superconductor. In the normal state at high temperatures, a magnetic field simply penetrates the material. In the superconducting state below T_c , the perfect diamagnetism (blue arrows) will assure that the magnetic induction $B = 0$ inside the superconductor. However, even if the material is cooled in an applied magnetic field (red arrows), the superconductor expels the applied field. Both effects are manifestations of the Meissner–Ochsenfeld effect, that, among others, can be used for the levitation of a superconductor in a magnetic field. The latter is illustrated by: (b) laboratory demonstration using a liquid nitrogen cooled high- T_c superconductor and a magnet, (c) a ‘toy train’ of the IFW Dresden equipped with a superconducting pellet, hovering above a magnetic track, and (d) Toyota/Lexus using the same technology to make “back-to-the-future” real. (e) Because of pinning (see later), it is even possible to make a tram “levitate” along a building or upside down as shown by this model at the KU Leuven.

phonons. The resulting electron pairs are called *Cooper pairs*. In most cases, the spins of the two electrons align antiparallel (spin singlets) and the angular momentum of the pair is zero (s-wave).

The Cooper pairs behave differently from single electrons which are fermions and have to obey the Pauli exclusion principle. In contrast, Cooper pairs are bosons. They condense into a single energy level which is slightly lower (a few meV, see Table 1) than the energy level of the normal state. Therefore an energy gap 2Δ separates the unpaired electrons (the so-called quasiparticles) from the Cooper pairs (Figure 3a). The energy gap automatically explains (i) the DC zero-resistance of the superconduc-

Table 1: Critical temperature T_c and zero temperature values of the energy gap Δ , Ginzburg–Landau coherence length ξ_{GL} , and critical fields B_c (for type-I superconductors) and B_{c2} (for type-II superconductors). Since the values vary in the literature, they should be taken as a guide only. For anisotropic superconductors, the subscripts (ab) and (c) refer to in-plane and out-of-plane properties, respectively. The subscript ‘max’ indicates the maximum reported value.

Material	T_c (K)	Δ (meV)	ξ_{GL} (nm)	λ_L (nm)	B_c, B_{c2} (T)
Al	1.2	0.17	1600	34	0.01 (B_c)
Pb	7.2	1.38	51–83	32–39	0.08 (B_c)
Nb	9.2	1.45	40	32–44	0.2 (B_c)
NbN	13–16	2.4–3.2	4	250	16
Nb ₃ Sn	18	3.3	4	80	24
Nb ₃ Ge	23.2	3.9–4.2	3–4	80	38
NbTi	9.6	1.1–1.4	4	60	16
YBa ₂ Cu ₃ O ₇	92	15–25 (max, ab)	1.6 (ab) 0.3 (c)	150 (ab) 800 (c)	240 (ab) 110 (c)
Bi ₂ Sr ₂ CaCu ₂ O ₈	94	15–25 (max, ab)	2 (ab) 0.1 (c)	200–300 (ab) > 15000 (c)	> 60 (ab) > 250 (c)
Bi ₂ Sr ₂ Ca ₂ Cu ₃ O ₁₀	110	25–35 (max, ab)	2.9 (ab) 0.1 (c)	150 (ab) > 1000 (c)	40 (ab) > 250 (c)
MgB ₂	40	1.8–7.5	10 (ab) 2 (c)	110 (ab) 280 (c)	15–20 (ab) 3 (c)
Ba _{0.6} K _{0.4} Fe ₂ As ₃	38	4–12	1.5 (ab) c > 5 (c)	190 (ab) 0.9 (c)	70–235 (ab) 100–140 (c)
NdO _{0.82} F _{0.18} FeAs	50	37	3.7 (ab) 0.9 (c)	190 (ab) c > 6000 (c)	62–70 (ab) 300 (c)

tor and (ii) the transition temperature, critical field, and other phenomena that restrict the superconducting regime, since it always requires an energy (thermal energy, magnetic field, current, or irradiation) of at least 2Δ to break a Cooper pair.

The BCS theory provides a number of valuable predictions. For instance, these include the temperature dependence of the energy gap (Figure 3c), the value of the energy gap at zero-temperature [9]:

$$\Delta(0\text{ K}) = 1.764k_B T_c, \quad (1)$$

and the dependence of the superconducting transition temperature T_c on the electron-phonon interaction V and the Debye frequency ω_D which, in the simplest form, is given by [7]

$$k_B T = 1.13\hbar\omega_D e^{-1/N(E_F)V}, \quad (2)$$

with k_B representing the Boltzmann constant and $N(E_F)$ the electronic density of states at the Fermi level. In the past, the latter equation suggested a possibility to optimize the transition temperature.

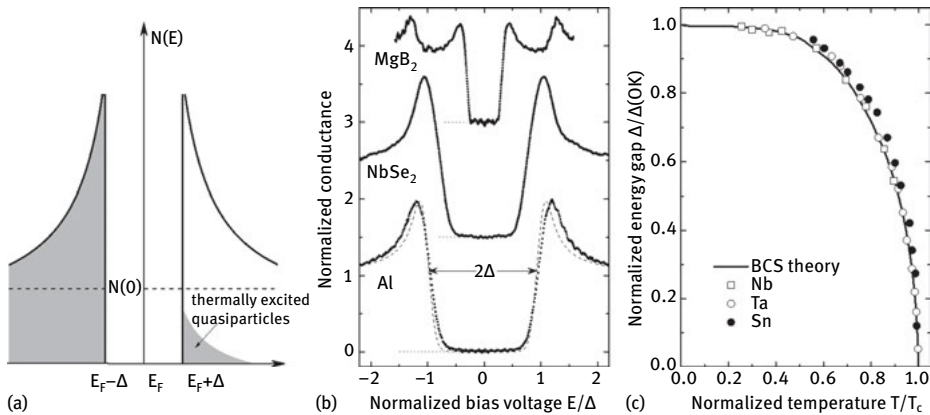


Fig. 3: (a) Schematic of the density of states at the superconducting energy gap, the shaded regime indicates the occupied states; (b) experimental verification obtained via scanning tunneling microscopy on various superconductors (see also Chapter 1), and (c) energy gap as function of reduced temperature according to the BCS theory (solid line) and for BCS-type superconductors (data from [8]). In (b) the data are normalized with respect to the energy gap Δ and, for better visibility, they are shifted with respect to the ordinate (gray dotted line represents zero conductance). Al and NbSe₂ show the ‘classic’ BCS behavior (for Al a BCS fit is added, dashed line), whereas MgB₂ represents a more complex superconductor with among others two energy gaps. For details of the tunnel spectroscopy and related topics refer to Chapter 1.

Many superconductors represent BCS-type superconductors (see Figure 3c) and even for the ‘non-BCS-type superconductors’ the general principles of the BCS theory are still valid. Nevertheless, we know now that the superconducting state can be much more complicated. This is especially the case for the much more complex new superconductors, like the high- T_c cuprates, MgB₂ (see Figure 3), pnictides, or even organic superconductors. Not only does Cooper pairing not really involve individual electrons pairing to form ‘quasibosons’, holes can also condensate to Cooper pairs, and d-wave superconductivity, p-wave superconductivity, multiband superconductivity, and coupling mechanisms other than phonon-mediated electron-electron interaction have to be taken into consideration to explain superconductivity in the more and more ‘exotic’ compounds. The careful analysis of the band structure of these materials is therefore a vital tool to understand these superconductors. A detailed discussion of this topic is given in Chapter 1.

4.2 Thermodynamic approach of Ginzburg and Landau

In contrast to the microscopic approach of the BCS theory, Ginzburg and Landau proposed a macroscopic description of superconductivity using universal thermodynamic arguments [10]. Their phenomenological theory was essentially correct when

they presented it in 1950 (i.e., prior to the BCS theory), however they assumed a charge $q = e$ of the superconducting charge carrier. With the appearance of the BCS theory, this charge was then replaced by the charge of the Cooper pair, $q = 2e$. Later, in 1959, Gor'kov demonstrated that the Ginsburg–Landau theory can be derived from the BCS theory [11].

Based on Landau's previously thermodynamic description of 2nd order phase transitions, Ginzburg and Landau argued that the free energy F of a superconductor near the superconducting transition can be expressed in terms of a complex order parameter ψ , which is zero in the normal state and nonzero in the superconducting state. Furthermore, ψ is related to the density of the superconducting charge n_s . Assuming that $|\psi|$ is small, the free energy can be expressed by

$$F - F_n = \alpha |\psi|^2 + \frac{\beta}{2} |\psi|^4 + \frac{1}{2m} \left| \left(\frac{\hbar}{i} \nabla - 2e\mathbf{A} \right) \psi \right|^2 + \frac{|\mathbf{B}|^2}{2\mu_0}, \quad (3)$$

with the parameters F_n representing the free energy in the normal phase, the phenomenological parameters α and β , m and $2e$ the effective mass and charge of the Cooper pair, and \mathbf{A} and \mathbf{B} the magnetic vector potential and magnetic field, respectively. Minimizing the free energy with respect to variations in the order parameter and the vector potential yields the important *Ginzburg–Landau equations*

$$\begin{aligned} \alpha\psi + \beta|\psi|^2\psi + \frac{1}{2m} \left(\frac{\hbar}{i} \nabla - 2e\mathbf{A} \right)^2 \psi &= 0, \\ \mathbf{j} = \frac{1}{\mu_0} (\nabla \times \mathbf{B}) &= \frac{2e}{m} \text{Re} \left\{ \psi * \left(\frac{\hbar}{i} \nabla + 2e\mathbf{A} \right) \psi \right\}, \end{aligned} \quad (4)$$

where \mathbf{j} denotes the electric current density and Re the real part. The first equation resembles the time-independent Schrödinger equation except for the nonlinear term. It determines the order parameter ψ , whereas the second equation provides the superconducting current.

The Ginzburg–Landau equations predict two important characteristic lengths in a superconductor, the coherence length ξ_{GL} and the penetration depth λ . The coherence length

$$\xi_{\text{GL}} = \sqrt{\frac{\hbar}{2m|\alpha|}} \quad (5)$$

characterizes the thermodynamic fluctuations in the superconducting phase. It is for instance manifested at a superconductor surface where the density n_s of Cooper pairs vanishes exponentially with a length scale of ξ_{GL} (Figure 4). Obviously, this parameter is temperature dependent. Moreover, it is correlated to the so-called BCS coherence length $\xi_0 = \hbar v_F / k_B T_c$ which characterizes the distance over which the two electrons forming a Cooper pair are correlated. Here v_F denotes the Fermi velocity.

The second parameter, the London penetration length λ , was already introduced by the London brothers in 1935 [29]. Expressed in terms of the Ginzburg–Landau model

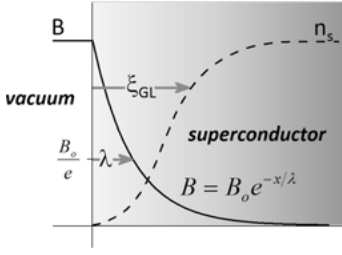


Fig. 4: Exponential decrease of the magnetic field and increase of the Cooper pair density at the surface of a superconductor define the London penetration depth λ and the Ginzburg–Landau coherence length ξ_{GL} .

it is given by

$$\lambda = \sqrt{\frac{m}{4\mu_0 e^2 \psi_0^2}}, \quad (6)$$

where ψ_0 is the equilibrium value of the order parameter in the absence of an electromagnetic field. The penetration depth sets the length scale according to which an external magnetic field decays exponentially inside the superconductor.

Finally, Ginzburg and Landau defined another parameter, the Ginzburg–Landau parameter $\kappa = \lambda/\xi_{GL}$, which plays an important role in the classification of superconductors with respect to their behavior in an applied magnetic field.

4.3 Type-I and type-II superconductors

The behavior of a superconductor in a magnetic field depends on two energy contributions: (i) the energy E_B that is necessary to expel the magnetic field from the superconductor and (ii) the energy E_C that is gained by the condensation of the Cooper pairs. Inside the superconductor both energies compensate each other, i.e., $-E_B = E_C = B_{c,th}^2/2\mu_0$ with the thermodynamic critical field $B_{c,th}$. However, at a S/N interface (superconductor to normal conductor interface) both energies are modified (see Figure 4), the magnetic field is not completely expelled and the Cooper-pair density is reduced. Therefore, the modification of these energies at a S/N interface with an area A is given by $\Delta E_B = A\lambda B_{c,th}^2/2\mu_0$ and $\Delta E_C = A\xi_{GL} B_{c,th}^2/2\mu_0$, respectively. As a consequence we obtain an energy contribution of a S/N interface of

$$\Delta E_C - \Delta E_B = (\xi_{GL} - \lambda) A B_{c,th}^2/2\mu_0, \quad (7)$$

which is positive for $\xi_{GL} > \lambda$ or negative for $\xi_{GL} < \lambda$. These different possibilities automatically give rise to different behaviors of the superconductor in an applied field. In one case S/N interfaces are energetically favored, in the other case not.

Exact calculations by Abrikosov in 1957 [12] predicted this behavior. He classified two types of superconductors according to their Ginzburg–Landau parameter. These superconductors are:

- *Type-I* for $\kappa < 1/\sqrt{2}$: Because of the positive energy necessary for the formation of S/N interfaces, these superconductors expel an applied magnetic field (except for

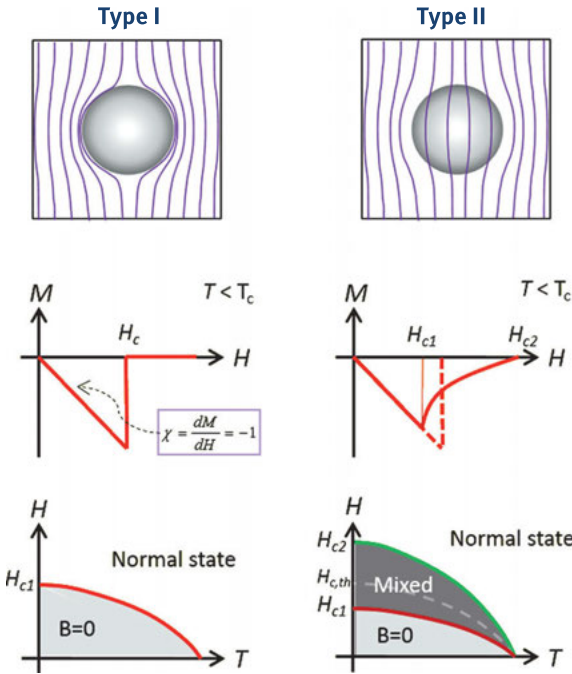


Fig. 5: Schematic sketches of the behavior of type-I and type-II superconductors in an applied magnetic field (top), magnetization in the superconducting state below T_c starting with ideal diamagnetism (Meissner phase with the magnetic susceptibility $\chi = -1$) followed by different types of field penetration (middle), and the resulting phase diagram with the Meissner state ($B = 0$), mixed state, and normal state separated by the different critical fields (bottom).

a thin layer at the surface) up to the critical field $H_c = H_{c,th}$. This is the Meissner–Ochsenfeld effect.

- *Type-II for $\kappa > 1/\sqrt{2}$:* These superconductors show a more complex behavior in an applied magnetic field. Only up to a first critical field H_{c1} is magnetic flux expelled. Above H_{c1} flux penetrates the superconductor since the formation of S/N interfaces are energetically favored. This phase is called the *mixed state* or *Shubnikov phase*. Nevertheless, superconductivity persists up to an upper critical field H_{c2} .

These different behaviors are shown in Figure 5.

In type-I superconductors the Meissner–Ochsenfeld effect takes place for fields below the critical field H_c . Above H_c the material becomes normal conducting (similar to the transition at T_c) and the magnetic field completely penetrates the superconductor, i.e., $M = 0$.

In contrast, type-II superconductors show a quite different behavior in a magnetic field:

- (i) The Meissner–Ochsenfeld effect ($B = 0$) is only present below the lower critical field H_{c1} .
- (ii) For higher fields, flux starts to penetrate the superconductor. However, superconductivity persists up the upper critical field H_{c2} and the magnetization is still finite ($M < 0$). The upper critical field is typically much larger than the critical field H_c or $H_{c,th}$ (see Table 1). This is one of the reasons why type-II superconductors are more suitable for technical applications.
- (iii) Moreover, since $(\Delta E_C - \Delta E_B) < 0$ the superconductor tries to form as many N/S surfaces as possible. Therefore, the flux penetrates in the form of magnetic *flux lines* that contain the smallest possible amount of magnetic flux, the magnetic flux quantum $\Phi_0 = h/2e = 2.07 \cdot 10^{-15}$ Wb. These flux lines (or fluxons) are quantum mechanical objects. They possess a normal conducting core of the size $2\xi_{GL}$, the magnetic field penetrating this normal core is surrounded by a superconducting current (see Figure 6). Because of this screening current these objects are also called vortices or *Abrikosov vortices*, taking into account their discoverer Abrikosov [12].
- (iv) Finally, the arrangement, shape, mobility, and motion of these vortices are all easily affected by a large number of interactions and energies. The major contributions to be considered are:
 - a. *Vortices-vortex interaction*: This interaction is repulsive. This can easily be understood by considering the interaction of the screening current of a vortex with the magnetic field of adjacent vortices. Already in 1957 Abrikosov predicted that the flux-lines would form a regular lattice. In an isotropic superconductor, this would be the closest 2D packing, i.e., a hexagonal or triangular lattice [12].
The first experimental proof of a periodic structure of the magnetic field in the mixed phase was obtained in 1964 using neutron diffraction which demonstrated the basic periodic structure of the magnetic field [13]. Real images of the *Abrikosov vortex lattice* were first observed in 1966 by Essmann and Trauble using a magnetic decoration technique [14].
However, small deviations and inhomogeneities, like anisotropic structural or superconducting properties or geometrical restrictions of the superconductor, can easily modify the structure of the (hexagonal) vortex lattice.
 - b. *Driving forces*: There are a number of forces and energies that can act as a driving force for the motion of vortices in a superconductor. Major candidates are the *Lorentz force* $\mathbf{F}_L = \mathbf{J} \times \Phi_0$ caused by any applied current, thermal energy, and gradients in temperature or magnetic field. The motion of vortices causes dissipation in the superconductor.
 - c. *Pinning force*: Fortunately, vortices can be ‘immobilized’ at defects in the material. This is called flux pinning or pinning.

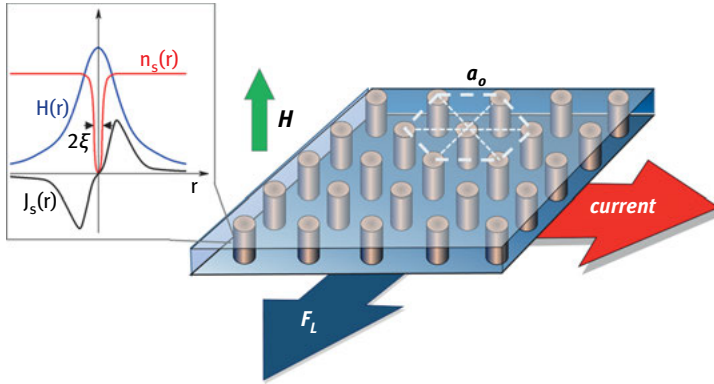


Fig. 6: Sketches of (left) a flux line with the radial distribution of the magnetic field H , the Cooper pair density n_s , and the circulating supercurrent J_s , and (right) the hexagonal flux line lattice with lattice parameter a_0 and arrows indicating the impact of an applied current on a flux line lattice leading to the Lorentz force F_L .

The complex interplay of the different interactions leads to the volume pinning force and, finally, to the critical current density that defines the dissipation-free current regime for type-II superconductors. Since its understanding, especially in the novel, highly complex superconductors as well as in nanostructured and artificially modified systems, represents a major topic of this book, we will briefly sketch the main aspects of this part of vortex matter.

4.4 Flux pinning and summation theory

In order to retain a dissipation-free DC current flow or reduce the voltage noise due to vortex motion, the flux lines have to be pinned by defects. The pinning force of the defects compensates the driving force up to a critical value. In the case of the Lorentz force F_L this defines the maximum dissipation-free current density, i.e., the critical current density J_c given by

$$\mathbf{F}_c = -\mathbf{F}_L = \mathbf{B} \times \mathbf{J}_c, \quad (8)$$

where F_c represents the volume pinning force which is obtained via summation of the elementary pinning forces f_p [15]. The elementary pinning force describes the individual interaction between a single vortex and a single inhomogeneity or defect in the superconducting material. It arises from the local modification of the superconductor by the defect that results in a local reduction of the energy associated with the vortex.

Possible defects can be classified according to their:

- *Elementary coupling mechanism*, such as *magnetic interaction* or *core interaction*: The magnetic interaction is essentially determined by the field gradient in the superconductor (i.e., the penetration length λ), whereas the core interaction

arises from the interaction of locally perturbed superconducting properties with the variation of the superconducting order parameter (i.e., the coherence length ξ). Since in technical type-II superconductors with large Ginzburg–Landau parameters κ the penetration length is much larger than the coherence length, core interactions are usually more effective pinning sites. There exist two predominant mechanisms of core pinning, which are δT_c and $\delta\kappa$ pinning. Whereas δT_c pinning is, for instance, caused by spatial variations in the Cooper-pair density, elasticity, or pairing interaction, $\delta\kappa$ pinning is predominantly caused by variations of the electronic mean free path.

- *Size or shape*: In order to contribute to the summation of individual pinning forces, the effective pinning site should be of the order of the local gradient. This implies that the pinning site should be smaller than ξ or λ for core pinning or magnetic interaction, respectively. Extended defects like surfaces, extended holes (e.g., so called antidots) or cones typically trap flux lines or even multiple flux quanta, i.e., quantized magnetic flux $\Phi = n\Phi_0$.
- *Origin*: Real superconductor materials always contain *natural defects* such as vacancies, precipitates, dislocation loops, stacking faults, or grain boundaries that contribute to the volume pinning. In most cases, several different types of natural pinning defects exist. However, one can also introduce *artificial pinning defects*. Typical candidates for thin film applications are irradiation defects or specially patterned defects like moats or channels [16] or small holes (so-called antidots) [17, 18]. Artificial pinning sites, their preparation and impact on various superconducting properties represents an important topic of this book (see Chapters 6 and 7).

As indicated above, the mechanism of flux pinning and, thus, the critical current density in real type-II superconductors is determined by (i) the *interaction between individual vortices* (VV interaction), (ii) the *interaction between individual pinning centers and vortices* f_p , (iii) the *driving force* (e.g., Lorentz force caused by an applied current, a field or temperature gradient or even a finite temperature), and (iv) the *homogeneity* of the superconducting material in terms of the amplitude and length scale of the variation of the superconducting properties. Therefore, a number of problems have to be solved in order to understand the range of effects caused by vortex motion in type-II superconductors [15]:

- First, the dominant class or classes of defects, which are responsible for the pinning, have to be determined and their elementary pinning forces f_p have to be computed.
- Second, the ‘response’ of the vortex lattice to the individual pin-vortex interactions has to be determined. For a small driving force (static vortex lattice) and small pinning forces, this can be for instance an elastic response described by the elastic matrix [19], plastic deformations, or instabilities [20]. The different mechanisms are comparable to the reaction of solids upon internal stresses. As long

as the strain is small the vortex lattice can reach its equilibrium position with respect to the pin distribution without plastic shear taking place in the lattice. In the case of larger strains plastic shear will create a significant number of defects in the vortex lattice. The deformation of the vortex lattice can be described by the displacement field. It can be two-dimensional (transversal displacement) [20] or three-dimensional [21].

- Third, the summation of the effects of many pins, usually at random position, leads to the prediction of the volume pinning force F_p that takes into account the elementary vortex interaction, the distribution and density of pinning sites, and the kind of deformation in the vortex lattice. Note that F_p is not automatically identical to the force $F_c = J_c B$, which is defined by the onset of vortex motion. The summation problem can be solved in some ideal or model systems. In the easiest case every pinning center is able to exert its maximum pinning force f_p on the vortex lattice, and the net volume pinning force F_p would be given by the direct summation, i.e., $F_c = F_p = \sum (f_p/V)$. This case is usually only observed in systems where individual flux lines are trapped by pinning sites, which is for instance the case for extremely small fields or superconductors with artificial defects. In all other cases the evaluation of the volume pinning force is more complex and requires summation in the formalism of the collective pinning theory [22].
- Finally, it is the mechanism of flux motion that determines the onset of dissipation and, therefore, the technically relevant critical current density $\mathbf{J}_c \times \mathbf{B} = \mathbf{F}_c$ with $F_c \leq F_p$, which is determined in the experiment. The volume critical force F_c can differ strongly from the volume pinning force F_p , which is evaluated for the case of elastic deformations. It depends upon (a) the relation between vortex-vortex and vortex-pin interactions and (b) the homogeneity of the superconductor on a length scale larger than the coherence length [23–26]. This automatically leads to two different mechanisms of vortex dynamics.

Pin breaking: If the differences between depinning forces of neighboring vortices are small compared to the vortex-vortex interaction, the complete vortex lattice will be pinned or depinned. This situation is referred to as pin breaking. The volume pinning is given by the statistical summation of the elementary interactions in the correlation volume $V_c = L_c R_c^2$ according to the collective pinning theory introduced by Larkin and Ovchinnikov [22]

$$F_c = F_p = \sqrt{\frac{n \cdot \langle f_p^2 \rangle}{V_c}} = \sqrt{\frac{W(0)}{V_c}}, \quad (9)$$

with n denoting the density of pinning sites, $W(0)$ representing the pinning parameter, and L_c and R_c the correlation lengths perpendicular and parallel to the magnetic field direction, respectively. The resulting field dependence is given in Figure 7. Up to a given field the elastic deformation of the vortex lattice is sustained and the field dependence of the volume pinning force is nicely described by the

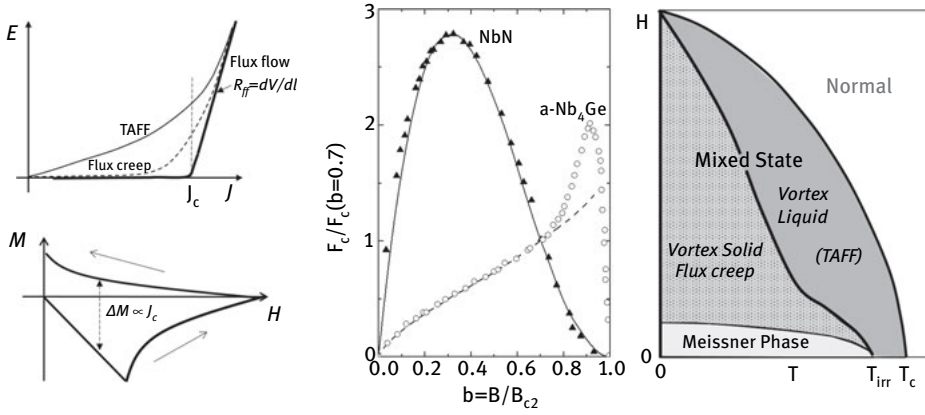


Fig. 7: The critical current is typically determined via resistive measurements (a) using a voltage criterion (typically $1 \mu\text{V}/\text{cm}$) or magnetic measurements (b) for which the pinning manifests itself by a hysteretic behavior. According to the Bean critical state model the difference ΔM in the magnetic measurement is proportional to the critical current density [27]. The resulting field dependence of the normalized volume pinning force is shown in (c) for a weak pinning amorphous Nb_4Ge thin film ($F_p(b = 0.7)$ typically of the order of 10^5 – 10^6 N/m^3 at 2.2 K) [20] and a strong-pinning NbN thin film ($F_c(b = 0.7)$ typically of the order of 10^8 – 10^9 N/m^3 at 4.2 K) [24] demonstrating pin-breaking according to the 2D collective pinning theory (dashed line) and the flux line shear mechanism (solid line), respectively. Finally, tunneling and thermal activation leads to the phase diagram (d) with a Meissner state (no vortices), a vortex solid with flux creep, and a vortex liquid with thermally activated flux flow (TAFF). The latter regime is more prominent for high- T_c materials.

equation above. At high fields close to B_{c2} , plastic deformations in the flux-line lattice set in leading to an increase of the pinning force with respect to the predictions of the collective pinning theory. The so-called peak effect at high fields (see Figure 7) is a characteristic feature of the collective pinning behavior in weak pinning materials.

Flux-line shear mechanisms: When the local pinning force strongly varies over length scales comparable to or larger than the vortex-vortex distance, vortices or bunches of vortices will start to move independently as soon as the driving force exceeds the flow stress of the vortex lattice. In this so-called flux-line shear mechanism, F_c is determined by the vortex-vortex interaction, it is not given by the volume pinning force F_p of the weak or strong pinning areas, respectively. Generally F_c should range between these two quantities, i.e., $F_{p,\text{strong}} > F_c > F_{p,\text{weak}}$. As a result, the volume pinning force is determined by the plastic shear properties of the vortex lattice, since areas that are weakly pinned shear away from strongly pinned regimes. The resulting volume pinning force is given by [23–26]

$$F_c = G \cdot c_{66} \propto \frac{B_{c2}^2}{w} b (1 - b)^2, \quad (10)$$

with c_{66} representing the shear modulus of the vortex lattice, G a geometrical factor that accounts for the orientation of the flux-flow channels with respect to the driving force, and $b = B/B_{c2}$ the reduced applied magnetic field. The typical field dependence obtained for strong pinning superconductors is shown in Figure 7. It is characterized by a broad peak at low field around $B \approx B_{c2}/3$. The flux-line shear mechanism is usually encountered in strong-pinning systems, whereas only weak-pinning superconductors show collective pinning behavior.

The field dependencies for pin breaking and flux-line shear given in Equations (9)–(10) and in Figure 7 refer to the ideal case of very homogeneous systems and low temperatures. Samples with a distribution of pinning properties or superconducting properties show deviations from these ideal behaviors. Moreover, up to now we did not take into account the impact of other energies on the vortex motion. Especially for the high- T_c superconductors the impact of thermal energy has to be considered.

4.5 Flux creep and thermally assisted flux flow

Although it was already discussed before, with the discovery of superconductivity it became evident that vortex motion for current densities $J < J_c = F_c/B$ has to be considered. Invoking a washboard-like pinning potential, individual vortices can tunnel (even at $T = 0$) or hop (e.g., thermally activated) from one potential well to the next one. This leads to two different behaviors which are, for instance, visible in the current-voltage characteristic (Figure 7a) and the phase diagram (Figure 7d).

Flux Creep: Tunneling of vortices was already predicted in 1962 and described later in the Kim-Anderson model for flux creep [30]. In this model, the tunneling rate of vortices is given by $R = \nu_0 \exp(-U/kT)$ where ν_0 is the attempt frequency (10^{-8} – 10^{-11} s^{-1}) and U the effective pinning potential (typically 10–1000 K). As a consequence an electric field is present already for $J < J_c$:

$$E = Bl\nu_0 \exp\left(-\frac{U}{kT}\left(1 - \frac{J}{J_c}\right)\right), \quad (11)$$

with l representing the average hopping distance. The resulting current-voltage characteristic shows a shallow increase of the electric field below J_c (Figure 7a), the technically relevant critical current is therefore smaller than J_c . Nevertheless, the flux creep regime in the mixed state represents a vortex solid state (Figure 7d).

Thermally Assisted Flux Flow: At elevated temperatures the impact of the thermal energy kT cannot be neglected. As a result, vortices cannot only tunnel, they can also hop from one well in the pinning potential to the next one. This hopping can occur in or even against the direction of the Lorentzian force. The resulting electric field is larger than the field generated by the tunneling of vortices, it is described in the so-

called thermally assisted flux flow model (TAFF) by [31]

$$E = 2Blv_0 \exp\left(-\frac{U}{kT}\right) \sinh\left(\left(\frac{U}{kT}\right)\left(1 - \frac{J}{J_c}\right)\right), \text{ and} \quad (12)$$

$$E(J \rightarrow 0) = J \cdot \left(2Blv_0 \frac{U}{J_c kT}\right) \equiv J \cdot \rho_{\text{TAFF}}.$$

As a result, flux motion leads to dissipation starting at zero current (Figure 7a) in the ‘TAFF’ regime of the mixed state, which therefore is called a vortex liquid state (Figure 7d). The vortex liquid state is separated from the vortex solid state by the so-called irreversibility line.

4.6 Josephson effects

Finally, we introduce one of the most intriguing effects in superconductivity, the *Josephson effects* named after their discoverer [32]. They are not only ideal manifestations of the macroscopic quantum-phenomenon of superconductivity, they also provide the basis for extremely sensitive devices that have revolutionized electromagnetic measurements. In general, the behavior of a tunneling junction (NIN, NIS, or SIS with N, I, and S denoting a normal metal, insulator, and superconductor, respectively) represent quantum-mechanical objects. Depending on the charge carriers, two different tunnel processes can be distinguished:

- (i) Tunneling of so-called quasiparticles (electrons or holes) was discovered by Giaever in 1960 [33]. In the case of superconductor tunnel junctions (SIS or NIS), the quasiparticle tunneling represents an ideal tool to determine the energy gap (see Figure 8, and Chapter 1).
- (ii) For the case of SIS junctions, additionally Cooper pairs can tunnel from one superconductor to the other. In contrast to the quasiparticle tunneling, where the tunneling is driven by a voltage difference between both conductors, the Cooper-pair tunneling is driven by the phase difference between the two superconductors. Since the phase difference can be constant (e.g., due to an applied magnetic field) or varying in time (due to a voltage difference between the superconductors) there exist two different effects, i.e., the DC Josephson effect and the AC Josephson effect, respectively [32].

Since the Josephson effects describe the behavior of superconductor tunnel junctions, we will briefly sketch the physics of tunneling in general before introducing the special effect of the tunneling of Cooper pairs.

4.6.1 Quasiparticle Tunneling

Tunneling through a barrier is only possible for quantum-mechanical particles, i.e., light particles like electrons. It can be described by the Schrödinger equation using the appropriate boundary conditions.

NIN tunnel junction: In NIN junctions, the tunneling current of the charge carriers (fermions) at a given voltage V and temperature is simply proportional to the tunneling probability T_n , the number of occupied states $D(E) \cdot f(E)$ of the normal conductor N_1 , and the number of unoccupied states $D(E + eV) \cdot (1 - f(E + eV))$ of the second normal conductor N_2 , into which the charge carriers tunnel. Here D and f represent the density of states and the Fermi–Dirac distribution, respectively. Via integration over the complete energy range and considering tunneling events in both directions, we obtain the resulting total tunneling current

$$\begin{aligned} I_{N_1N_2} &= \frac{2\pi e}{\hbar} |T_n|^2 \int_{-\infty}^{\infty} D_{N_1}(E) D_{N_2}(E + eV) (f(E) - f(E + eV)) dE \\ &\approx \frac{2\pi e}{\hbar} |T_n|^2 D_{N_1}(E_F) D_{N_2}(E_F) eV \equiv G_{N_1N_2} V \equiv \frac{1}{R_{N_1N_2}} V. \end{aligned} \quad (13)$$

For the NIN junction the resulting current-voltage characteristic is simply ohmic (Figure 8a), i.e., $I \propto V$ with a proportionality factor given by the conductance G_{NIN} or the inverse resistance $1/R_{NIN}$.

NIS tunnel junction: Because of the energy gap 2Δ of the superconductor, the case of the NIS junction is a bit more complex (Figure 8b). Around the energy gap, the density of states of the normal charge carriers (fermions which due to their particle-like behavior are called quasiparticles) in a superconductor is given by:

$$\begin{aligned} D_S(E) &= D_N(E_F) \frac{E}{\sqrt{E^2 - \Delta^2}} \quad \text{for } |E| \geq \Delta \\ &= 0 \quad \text{for } |E| < \Delta, \end{aligned} \quad (14)$$

with $E_F := 0$. In analogy to the NIN junction the NIS tunnel current is given by:

$$\begin{aligned} I_{NIS} &= \frac{2\pi e}{\hbar} |T_n|^2 \int_{-\infty; \text{for } |E| > \Delta}^{+\infty} D_N(E) D_S(E + eV) (f(E) - f(E + eV)) dE \\ &\approx \frac{G_{NIN}}{e} \int_{-\infty}^{\infty} \frac{|E|}{\sqrt{|E^2 - \Delta^2|}} (f(E) - f(E + eV)) dE. \end{aligned} \quad (15)$$

For zero temperature and assuming a constant (i.e., energy independent) density of states around the Fermi level, this simplifies to:

$$\begin{aligned} I_{NIS} &= 0 \quad \text{for } |eV| < \Delta \ll E_F \\ &= \frac{G_{NIN}}{e} \sqrt{|(eV)^2 - \Delta^2|} \quad \text{for } |eV| \geq \Delta \ll E_F. \end{aligned} \quad (16)$$

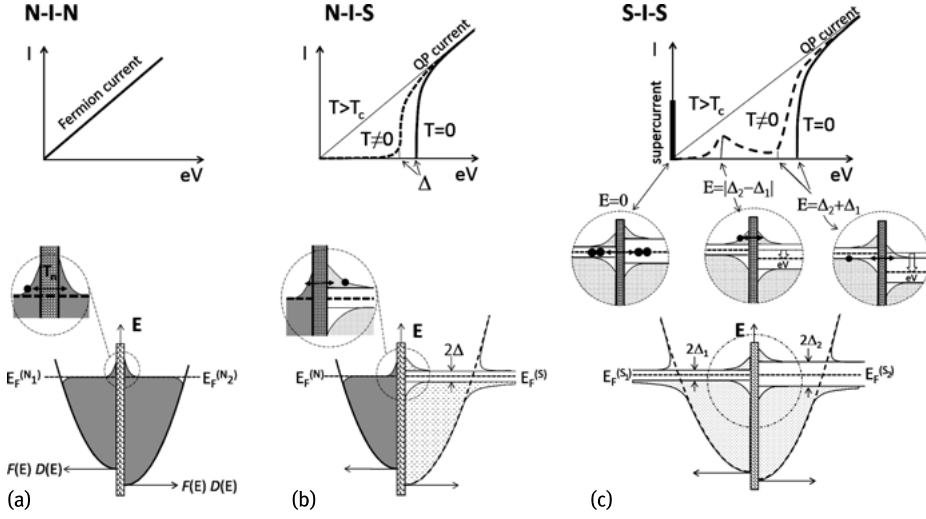


Fig. 8: Schematic diagrams of the current voltage characteristic (top) and density of states at the Fermi level (bottom) of a NIN (a), NIS (b), SIS (c) junction showing the tunneling events of the different contributions of the Fermi current (NIN), quasiparticles (NIS and SIS), and Cooper pairs (SIS). The insets show close-ups of the different tunnel events.

The resulting current voltage characteristics are shown in Figure 8b. For zero temperature, the onset of current occurs at $eV = \Delta$ ($T = 0$), at higher voltages the characteristic asymptotically approaches a linear behavior defined by the conductivity G_{NIN} . With increasing temperature the energy gap decreases (see also Figure 3a) and thermal activation leads to tunneling of the quasiparticles also for voltages $eV < \Delta(T)$. As a result the characteristics recorded at finite temperature are smeared out as indicated in Figure 8b. Nevertheless, the highly nonlinear behavior allows one to determine the energy gap $\Delta(T)$ as discussed in Chapter 1.

SIS tunnel junction: In principle, the SIS junction can be treated in an analogous way. The quasiparticle tunneling is given by:

$$\begin{aligned}
 I_{S_1 S_2} &= \frac{2\pi e}{\hbar} |T_n|^2 \int_{-\infty; \text{for } |E| > \max\{\Delta_1, \Delta_2\}}^{+\infty} D_{S_1}(E) D_{S_2}(E + eV) (f(E) - f(E + eV)) dE \\
 &\approx \frac{G_{N_1 N_2}}{e} \int_{-\infty}^{\infty} \frac{|E|}{\sqrt{|E^2 - \Delta_1^2|}} \frac{|E|}{\sqrt{|(E + eV)^2 - \Delta_2^2|}} (f(E) - f(E + eV)) dE. \quad (17)
 \end{aligned}$$

However, the evaluation is quite complex, even for $T = 0$ K. Nevertheless, the current voltage characteristic can be obtained by considering a simple graphical representation of the density of states as sketched in Figure 8c.

4.6.2 Cooper Pair Tunneling

Up to now, we only considered the tunneling of the quasiparticles. However, already in 1962 Josephson predicted [32] that (i) Cooper pairs might also participate in the tunneling process and (ii) that due to the macroscopic quantum state of the superconductor this might result in some spectacular effects. Only one year later in 1963, the predictions were experimentally verified [34].

Since the tunneling of Cooper pairs is driven by the phase difference between the two superconductors and not by a voltage difference as in the case of quasiparticle tunneling, it is already present for $V = 0$. In general, Cooper pairs in a superconductor are quantum mechanical objects. They can be described by the time-dependent Schrödinger equation $i\hbar\partial\Psi/\partial t = E\Psi$ with the wave function $\Psi = |\Psi|e^{i\phi}$, the phase ϕ , and the superconducting condensate density $n_s = |\Psi|^2$. With a tunneling frequency T of the Cooper pairs, an applied voltage V between the two superconductors S_1 and S_2 , the charge of the Cooper pairs $q = 2e$, and a definition of the zero-energy reference $E_F := 0$, the basic set of equations which describe the tunneling of the Cooper pairs is given by

$$\begin{aligned} i\hbar\frac{\partial\Psi_1}{\partial t} &= \hbar T\Psi_2 - eV\Psi_1 \\ i\hbar\frac{\partial\Psi_2}{\partial t} &= \hbar T\Psi_1 + eV\Psi_2 . \end{aligned} \quad (18)$$

Equation (18) shows that the condensate density $n_s = |\Psi|^2$ in S_1 is increased by the tunneling of Cooper pairs from S_2 , and vice-versa. Furthermore, the difference in energy between S_1 and S_2 is given by $(2e)V$, which for mathematical reasons is symmetrized over the two superconductors. Assuming identical superconductors (i.e., $n_s \approx n_s(S_1) \approx n_s(S_2)$), Equation (18) leads to expressions for the phase difference between the two superconductors and the superconducting tunneling current J

$$\frac{\partial(\phi_2 - \phi_1)}{\partial t} = -\frac{2e}{\hbar}V \quad \text{or:} \quad \Delta\phi = \phi_2 - \phi_1 = -\frac{2e}{\hbar}Vt + \text{const.} , \quad (19)$$

with $2eV/\hbar = \omega$ representing an angular frequency, and

$$J(t) = \frac{\partial n_s(S_1)}{\partial t} = -\frac{\partial n_s(S_2)}{\partial t} = Tn_s \sin(\Delta\phi) = J_0 \sin(\gamma_0 - \omega t) . \quad (20)$$

These two expressions automatically lead to the two different Josephson effects.

DC Josephson effect: For zero-voltage, the tunneling current is simply determined by the phase difference between the two superconductors:

$$J = J_0 \sin(\Delta\phi) . \quad (21)$$

Since $V = 0$, this phase difference is constant in time. However, it can be modified by an applied magnetic flux in the junction. As a result, the tunneling current varies in a sinusoidal way upon the applied magnetic field. This effect is, for instance, used

in extremely sensitive magnetic field sensors, superconducting quantum interference devices (SQUID). A detailed report on recent developments on NanoSQUIDs is given in Chapter 11.

AC Josephson effect: For voltages $V \neq 0$, the phase varies in time and we automatically obtain an AC tunneling current with a voltage-dependent frequency:

$$f_J = \frac{2e}{h} V. \quad (22)$$

The maximum voltage that can be applied to the tunnel junction is given by $V_{\max} = \Delta/(2e)$. Therefore, the maximum frequency that can be generated by the Josephson junctions is $f_{J,\max} = \Delta/h$. For Al, Nb, and BSCCO, with gaps of 0.17 meV, 1.45 meV, and ~ 25 meV (see Table 1), the maximum frequencies are 82 GHz, 700 GHz, and 12 THz, respectively. This demonstrates that the AC Josephson effect represents a relatively easy way to generate or detect GHz and even THz frequencies. In the latter case, an AC signal would directly be converted to a voltage signal.

This principle became even more attractive with the discovery of the intrinsic Josephson effect in the highly anisotropic high- T_c superconductors in 1992 [35]. Because of the high anisotropy and short coherence length compared to the lattice spacing between the superconducting CuO planes in $\text{Bi}_2\text{Sr}_2\text{CaCu}_2\text{O}_8$, the 2D superconducting layers are seemingly intrinsically separated by an ‘insulating layer’. In this way they form stacks of natural (i.e., intrinsic) SIS junctions. In the meantime, the intrinsic Josephson effect has been observed in a number of other systems. Since these SIS stacks form naturally and since the AC Josephson current density is potentially very high, these systems are very promising candidates for various GHz to THz applications. Recent developments in this field are reviewed in Chapter 12.

5 Application of superconductivity

In the previous sections, we introduced the basic aspects of the quantum mechanical phenomenon called superconductivity. We demonstrated that the macroscopic quantum state of the Cooper pairs results in:

- (i) *perfect conductivity* resulting in zero-resistance $\rho = 0$ at dc current and a very small microwave surface resistance at high frequencies;
- (ii) *perfect diamagnetism* (Meissner–Ochsenfeld effect);
- (iii) *quantization of magnetic flux* resulting in the formation of single-quanta (or multiquanta) vortices that interact with each other and with defects in the superconductor, and;
- (iv) *phase correlation* of the charge-carrier wave function which in weak-link structures leads to the Josephson effects.

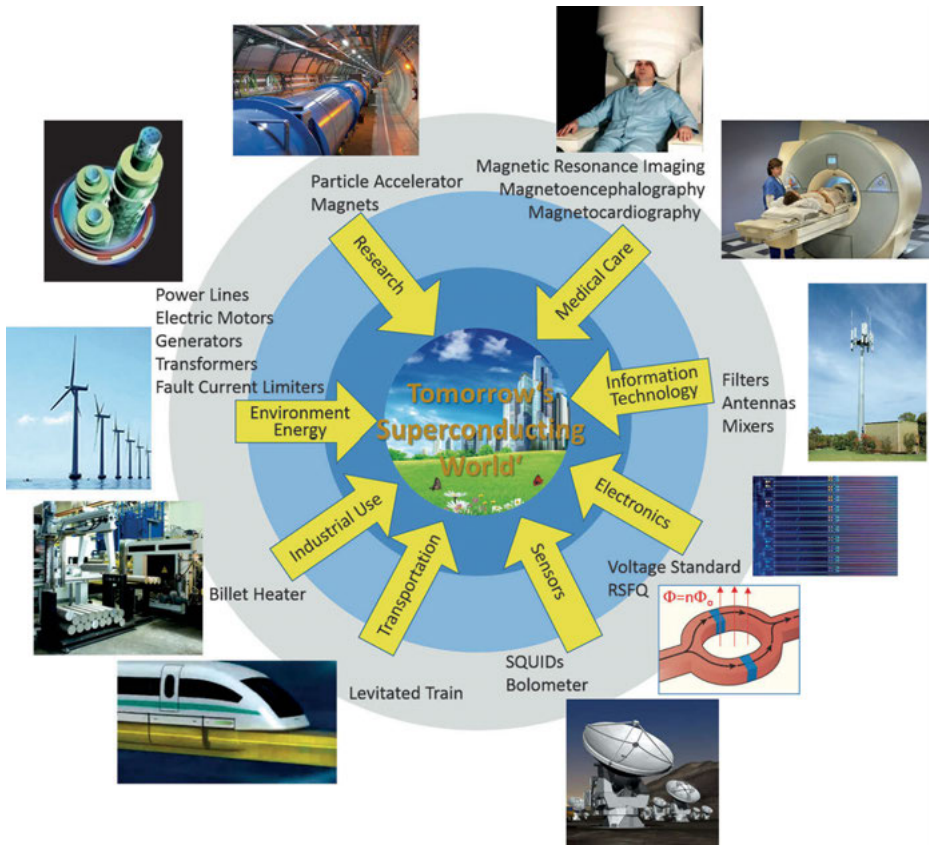


Fig. 9: 'Tomorrows Superconducting World' shows where we already benefit from superconductivity or could benefit from it in the future.

These extraordinary properties mean that superconductivity offers a high potential for improvement of existing applications or even novel applications in various fields. Existing, relatively well-established applications are (Figure 9):

- **Medical care:** A number of diagnostic superconductor applications are well established in medical care. Magnetic resonance imaging (MRI) is widely used for visualizing organs and structures inside the human body. Similarly, magnetoencephalography (MEG) is used for analysis of the brain and brain activities. Other applications are feasible, e.g., magnetocardiography (MCG) measuring the magnetic activity of the heart could become the counterpart to electrocardiography (ECG).
- **Information technology, electronics, and sensors:** Superconductivity bears the potential to improve quite a number of technologies. For instance, superconducting filters, antennas, and mixers can improve the performance of the data

transmission and data handling of base stations for cell phones. Even complex ultrafast electronics, the so-called ‘software radio’ is being considered for the improvement of data handling in devices like base stations.

The extreme magnetic field sensitivity of the so-called Superconducting Quantum Interference Device (SQUIDs) is used for various kinds of highly sensitive sensors (e.g., magnetometers, amplifiers, current meters, and particle detectors). Superconducting bolometers are well established in radio astronomy. They could also become attractive for other bolometric applications.

Finally, complex circuits based on Josephson arrays could be used for various electronic applications ranging from standards (e.g., voltage standards) and logic devices, to quantum computing (e.g., Rapid Single Flux Quantum Logic, RSFQ).

- Environment, energy, industrial use, and transportation: The majority of applications in this field is based on the use of superconducting cables. On the one hand, superconducting cables can be used in power lines leading to a significant reduction of the losses. On the other hand, wound into coils they can be used in high-field magnets or electric motors and generators. The superconducting billet heater represents an example for the use of superconducting magnets for industrial application. Superconducting motors or generators benefit from their large power density, which could be used to enhance the power or reduce the volume and mass of the device. This would be very attractive for larger engines or generators, like ship’s engines, hydro or wind turbines.
- Research: Last but not least, superconductor applications are well established in various fields of contemporary research. Outstanding examples are particle accelerators and fusion reactors. However, high-field magnets, imaging technologies (e.g., nuclear resonance imaging), or superconducting sensors (e.g., SQUIDs or bolometers) are also successfully used in many laboratories.

6 Superconductors at the nanoscale

The list above (see also Figure 9) demonstrates that there are quite a number of well-established applications of superconductivity. However, there are even more less-established or potential applications that either benefit from the use of superconductivity or are only feasible due to superconductivity. In order to develop the full potential of superconductors, it is essential to analyze, understand, engineer, and optimize them at the nanoscale. There are a number of very important questions and problems that are worth examining in this context (see also Figure 10):

- Improvement of superconductors, critical parameters: The critical parameters T_c , B_{c2} , and J_c define the operating regime. The enhancement of these critical parameters is one aim of superconductor research. The search for systems with higher transition temperatures, if possible even ‘room temperature superconduct-

tivity', is definitely the research that attracts the most publicity. Nevertheless, it depends on the kind of application and which of the critical parameters represents a restriction and should be increased (typically, J_c and B_{c2} for high-field applications, J_c for low-field applications). Whereas T_c and B_{c2} represent material-specific parameters, J_c depends on the defects (type, density, arrangement) in the superconductor. Thus, in the first case, research on new superconductors is required. In the latter case, the role of pinning sites (i.e., type of defect, defect density and distribution) has to be analyzed, understood, and optimized. The introduction of pinning sites can be affected by the preparation process of the superconductor. However, they can also be introduced artificially after or during growth. In both cases this requires manipulation of the material on the scale of the coherence length, i.e., at the nanoscale.

- Vortex matter and fluxonics: The vortices and vortex lattice are not only quantum mechanical objects, they are also ideal nano-objects. Vortices possess a normal core of $\sim 2\xi$. As indicated above, pinning sites of nanometer size are required for optimized pinning of these vortices. However, the lattice parameter is also of nanometer size. Moreover, it can be varied over a large range by varying the applied field. An undistorted hexagonal vortex lattice has a lattice parameter $a_0 = 1.15(\Phi_0/B)^{1/2}$, i.e., a_0 varies from 166 nm to 53 nm to 17 nm for 100 mT, 1 T, and 10 T, respectively. Regular arrays of pinning sites (natural or artificial) can be used to achieve commensurability or matching between the vortex lattice and the pinning array. Moreover, subtle arrangements of pinning defects can be used for novel fluxonic concepts (e.g., flux guidance, vortex ratchets, vortex transistors) or improvement of existing device concepts (e.g., noise reduction in SQUIDs, frequency tuning of filters and antennae).
- Josephson physics: The second obvious nano-objects are tunnel junctions leading to the Josephson effects. The fabrication of the nanosized barrier between the two superconductors is highly demanding, especially if several (two junctions per dc SQUID, thousands for complex electronic circuits like voltage standards or RSFQ) identical tunnel junctions are required. Moreover, due to the miniaturization of electronics and sensors the fabrication of the individual device components require a reliable and reproducible preparation at the nanoscale.
- Anisotropy, 2D structure of high- T_c materials: Most applications still operate at 4 K, which requires liquid-He cooling or quite expensive cryocooling. The discovery of the high- T_c superconductors opened the temperature window for less-expensive operation using liquid nitrogen at 77 K or simpler cryocoolers. However, the enhancement of T_c has been achieved by a higher complexity of the superconductor, a 2D layered structure, and an extremely small coherence length (e.g., $\text{YBa}_2\text{Cu}_3\text{O}_7$ with $\xi_{ab} \approx 1.6$ nm and $\xi_c \approx 0.3$). Thus, the 2D nature and the small coherence length generally require additional engineering of these complex materials at the nanoscale.

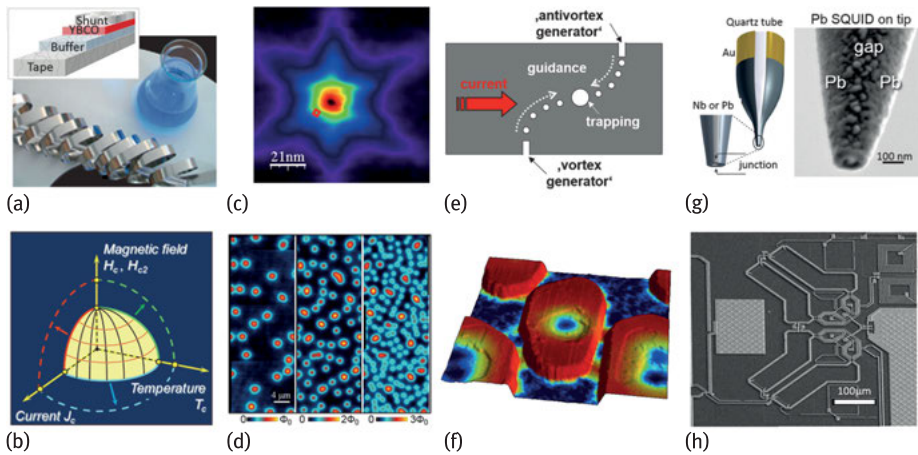


Fig. 10: Some of the strategies in the research on ‘*Superconductors at the Nanoscale*’ that are discussed in this book. (a) Chemical deposition of high- T_c films as an example for the development of improved or novel preparation technologies, for instance, for HTS coated conductors (see Chapter 6), (b) improvement of critical properties of existing superconductors and search and understanding of novel superconductors, (c) analysis and visualization of nanophysics in superconductors (here: microscopy on a single vortex) (see Chapter 1), (d) analysis of interactions and collective phenomena on the nanoscale, (here: coexistence of single and multiquanta vortices) (see Chapters 4 and 5), (e) development of novel concepts to manipulate superconducting properties at the nanoscale (here: fluxonic concept for vortex manipulation via nanoscale patterning) (see Chapter 7), (f) examination of the physics in superconductors at extremely small scales (here: granularity, superconductivity, Josephson behavior in nanosize superconducting islands) (see Chapter 3), (g) novel nanosize applications (here: NanoSQUID on a tip) (see Chapters 9–15), and (h) complex devices composed of nanosize components (here: SQUID-based microsusceptometer) (see Chapters 11–15).

- **Combination of superconductors and nonsuperconductors:** In the end, the superconductor has to be connected to the ‘outer world’, i.e., to nonsuperconducting materials. Moreover, the combination with nonsuperconducting material might provide novel and interesting properties. This is, for instance, the case for superconductor-ferromagnetic hybrid systems. In all cases, the small superconductor coherence length requires an understanding and optimization of the interface between the superconductor and the nonsuperconductor at the nanometer scale.

It is the aim of this book to provide an overview of the state of research and novel approaches for the questions and problems that are addressed above. It comprises an up-to-date view on the research and a contemporary perspective on ‘*Superconductors at the Nanoscale*’.

Bibliography

- [1] Kamerlingh-Onnes H. *Proc. R. Acad. Amsterdam* 11:168, 1908.
- [2] Kamerlingh-Onnes H. *Commun. Leiden, Suppl. Nr. 34*, 1913.
- [3] Bednorz JG, Müller KA. *Z. Phys. B* 64:189, 1986.
- [4] Wu MK, Ashburn JR, Torng CJ, Hor PH, Meng RL, Gao L, Huang ZJ, Chu CW. *Phys. Rev. Lett.* 58:908, 1987; Zhao ZX. *Int. J. Mod. Phys. B* 1:179, 1987.
- [5] Nagamatsu J, Nakagawa N, Muranaka T, Zenitani Y, Akimitsu J. *Nature* 410:63, 2001.
- [6] Takahashi H, Igawa K, Arii K, Kamihara Y, Hirano M, Hosono H. *Nature* 453:376, 2008.
- [7] Bardeen J, Cooper LN, Schrieffer JR. *Phys. Rev.* 108:1175, 1957.
- [8] Townsend P, Sutton J. "Investigation by Electron Tunneling of the Superconducting Energy Gaps in Nb, Ta, Sn and Pb," *Phys. Rev.* 128(2):591–595, 1962.
- [9] Tinkham M. *Introduction to Superconductivity*. Dover Publications, 1996, p. 63.
- [10] Ginzburg VL, Landau LD. *Zh. Eksp. Teor. Fiz.* 20:1064, 1950. English translation in: Landau LD. *Collected papers*. Oxford: Pergamon Press, 1965, p. 546.
- [11] Gor'kov LP. *Sov. Phys. JETP* 36:1364, 1959.
- [12] Abrikosov AA. *Zh. Eksp. Teor. Fiz.* 32:1442, 1957 (English translation: *Sov. Phys. JETP* 5:1174, 1957).
- [13] Cribier D, Jacrot B, Madhav Rao L, Farnoux B. *Phys. Lett.* 9:106, 1964.
- [14] Essmann U, Trauble H. *Phys. Lett. A* 24:526, 1967; *J. Sci. Instrum.* 43:344, 1966.
- [15] Wördenweber R. *Rep. Prog. Phys.* 62:187–236, 1999.
- [16] Pruymboom A, Kes PH, van der Drift E, Radelaar S. *Phys. Rev. Lett.* 60:1430, 1988.
- [17] Baert M, Metluskov VV, Jonckheere R, Moshchalkov VV, Bruynseraede Y. *Phys. Rev. Lett.* 74:3269, 1995.
- [18] Castellanos AM, Wördenweber R, Ockenfuss G, v.d. Hart A, Keck K. *Appl. Phys. Lett.* 71:962, 1997.
- [19] Brandt EH. *Phys. Stat. Sol. B* 77:551, 1976; *J. Low Temp. Phys.* 26:709 and 735, 1977; *J. Low Temp. Phys.* 28:263 and 291, 1977.
- [20] Wördenweber R, Kes PH, Tsuei CC. *Phys. Rev. B* 33:3172, 1986.
- [21] Wördenweber R, Kes PH. *Phys. Rev. B* 34:494, 1986.
- [22] Larkin AI, Ovchinnikov YuN. *J. Low Temp. Phys.* 34:409, 1979.
- [23] Kramer EJ. *J. Nucl. Mater.* 72:5, 1978.
- [24] Pruymboom A, Kes PH, van der Drift E, Radelaar S. *Appl. Phys. Lett.* 52:662, 1988.
- [25] Welch DO. *J. of Adv. Science* 4:81, 1992.
- [26] Wördenweber R. *Phys. Rev. B* 46:3076, 1992.
- [27] Bean CP. *Magnetization of high-field superconductors*, *Phys. Rev. Lett.* 8:250, 1962; *Rev. Mod. Phys.* 36:31, 1964.
- [28] Meissner W, Ochsenfeld R. *Naturwissenschaften* 21:787, 1933.
- [29] London F, London H. *Z. Phys.* 96:359, 1935; London F. *Une conception nouvelle de la supraconductivité*, Hermann and Cie, Paris, 1937.
- [30] Anderson PW. *Phys. Rev. Lett.* 9:309, 1962; Anderson PW, Kim YB. *Rev. Mod. Phys.* 36:39, 1994.
- [31] Kes PH, Aarts J, van den Berg J, van der Beek CJ, Mydosh JA. *Supercond. Sci. Technol.* 1:242–248, 1989.
- [32] Josephson BD. "Possible new effects in superconductive tunnelling," *Phys. Lett.* 1:251, 1962; "The discovery of tunnelling supercurrents". *Rev. Mod. Phys.* 46:251, 1974.
- [33] Giaever I. "Energy Gap in Superconductors Measured by Electron Tunneling", *Phys. Rev. Lett.* 5:147–148, 1960; Giaever I. "Electron Tunneling Between Two Superconductors". *Phys. Rev.*

- Lett. 5:464, 1960; Giaever I. "Electron tunneling and superconductivity". Rev. of Modern Phys. 46:245, 1974.
- [34] Rowell JM, Anderson PW, Thomas DE. Image of the Phonon Spectrum in the Tunneling Characteristic between Superconductors. In: Phys. Rev. Lett. 10:334, 1963.
- [35] Kleiner R, Steinmeyer F, Kunkel G, Müller P. Intrinsic Josephson effects in Bi2Sr2CaCu2O8 single crystals, Phys. Rev. Lett. 68:2394, 1992.

